

**SYNTHESIS, CHARACTERIZATION AND CATALYTIC
ACTIVITY OF MCM-41 IMIDAZOLIUM HALIDE
CATALYSTS FOR THE REACTION BETWEEN
EPOXIDES AND CARBON DIOXIDE**

JIMMY NELSON A/L APPATURI

UNIVERSITI SAINS MALAYSIA

2015

**SYNTHESIS, CHARACTERIZATION AND CATALYTIC
ACTIVITY OF MCM-41 IMIDAZOLIUM HALIDE
CATALYSTS FOR THE REACTION BETWEEN
EPOXIDES AND CARBON DIOXIDE**

by

JIMMY NELSON A/L APPATURI

**Thesis submitted in fulfillment of the requirements
for the degree of
Doctor of Philosophy**

January 2015

ACKNOWLEDGEMENTS

I would like to express my immense gratitude to my supervisor, Professor Dr. Farook Adam, for his guidance and constant support throughout my research period. I am also thankful to USM for the funds to conduct this research through RU Grant (Ac. No.: 1001/PKIMIA/814127) and providing financial assistance through Postgraduate Research Grant Scheme (PRGS) (Ac. No.: 1001/PKIMIA/844075). I would also like to thank the Malaysian Government for a FRGS Grant (Ac. No.: 203/PKIMIA/6711316). Heartfelt thanks and appreciation goes to Ministry of Education for providing me with a scholarship through the MyBrain15 program.

I am very grateful to my parents, brothers, relatives, and my special person, Ms. Thiruchelvi Pulingam for their moral support, prayers, constant encouragement and understanding throughout my difficult times in USM. My gratitude also goes to the staff of the School of Chemical Sciences, School of Biological Sciences and School of Physics for their help in the use of the necessary equipments and analysis.

I wish to express my warm and sincere thanks to all my best colleagues and friends. Thank you Dr. Radhika Thankappan (Post Doctoral Fellow), Dr. Zakia Khanam (Post Doctoral Fellow), Dr. Anwar Iqbal, Dr. Kassim Mohammed Heloo, Dr. Ishraga Abdelmoniem Hassan, Dr. Abbas, Dr. Mohammad, Dr. Tammar Hussein Ali, Dr. Kueh Chien Wen, Salih, Chew Thiam Seng, Sek Kei Lin, Wong Jia Tian, Hiba Eltahier Hassan, Wong Min Siang, Ooi Wan Ting, Siti, Atikah and

Lingeswarran Muniandy who gave me confidence, help and support. Special thanks to my best friends Dr. Jeyashelly Andas and Dr. Muazu Samaila Batagarawa for helping me throughout the research period.

I wish to thank my friends, especially those who are involved with me in *Persatuan Graduan Pelajar India Institusi Pengajian Tinggi, Daerah Kuala Muda, Kedah* (GAPIT) for thier love, encouragement and full support in every stage of my research work.

TABLE OF CONTENTS

	Page
ACKNOWLEDGEMENTS	ii
TABLE OF CONTENTS	iv
LIST OF TABLES	xi
LIST OF FIGURES	xiii
LIST OF SCHEMES	xix
LIST OF APPENDICES	xxi
LIST OF SYMBOLS AND ABBREVIATIONS	xxiii
ABSTRAK	xxvii
ABSTRACT	xxix
CHAPTER 1 – INTRODUCTION	1
1.1 Global warming	1
1.2 Carbon dioxide	2
1.2.1 The use of CO ₂ as C1 building block	3
1.2.2 Synthesis of cyclic carbonate	5
1.3 Role of catalysts in the production of cyclic carbonates	7
1.3.1 Heterogeneous ionic liquid catalyst	8
1.4 Factors influencing the production of cyclic carbonates	10
1.4.1 Influence of temperature	14
1.4.2 Influence of pressure	15
1.4.3 Influence of solvent	17
1.5 The mechanism of cycloaddition of CO ₂ to epoxides	19
1.5.1 Ring opening of epoxide	19
1.5.2 Activation of CO ₂	23

1.6	Rice Husk	27
1.6.1	Utilization of rice husk ash	28
1.6.2	RHA as a catalyst support	30
1.7	Silica and M41S family	31
1.7.1	MCM-41	33
1.7.2	The organic functionalization on MCM-41	34
1.7.2.1	Grafting method	35
1.7.2.2	Co-condensation method	36
1.7.2.3	Periodic mesoporous organosilanes (PMOs)	38
1.7.3	The application of MCM-41	40
1.8	Problem statements	41
1.9	Objectives of the present work	42
CHAPTER 2 – MATERIALS AND METHODS		44
2.1	Raw material and chemicals	44
2.2	Extraction of silica from RH	46
2.2.1	Washing and pretreatment of RH	46
2.2.2	Preparation of sodium silicate solution	46
2.3	Preparation of the catalysts	46
2.3.1	Preparation of mixed surfactant solution	46
2.3.2	Preparation of MCM-41	47
2.3.3	Preparation of Cl-MCM-41	47
2.3.4	Synthesis of MCM-41-Imi	48
2.3.5	Synthesis of MCM-41-Imi/Br	48
2.3.6	Synthesis of MCM-41-Imi/Cl and MCM-41-Imi/I	49
2.4	Catalyst characterization	50

2.4.1	Surface characterization	50
2.4.1.1	Fourier Transform Infrared Spectroscopy (FT-IR) analysis	50
2.4.1.2	Nitrogen adsorption - desorption analysis	50
2.4.1.3	²⁹ Si CP/MAS NMR spectroscopic analysis	51
2.4.1.4	¹³ C CP/MAS NMR spectroscopic analysis	51
2.4.1.5	Scanning Electron Microscopy (SEM) / Energy Dispersive X-ray Spectroscopy (EDS)	52
2.4.1.6	Transmission Electron Microscopy (TEM)	52
2.4.2	Bulk characterization	53
2.4.2.1	Ion chromatography analysis	53
2.4.2.2	Redox titration	53
2.4.2.3	Powder X-Ray Diffraction (XRD)	54
2.4.2.4	Carbon, Hydrogen, Nitrogen (CHN) analysis	55
2.4.2.5	Thermogravimetric analysis (TG-DTG)	56
2.5	Catalytic reaction	57
2.5.1	High pressure autoclave reactor	57
2.5.2	Procedure of the insertion reaction	59
2.5.3	Influence of reaction conditions	59
2.5.4	Product analysis and identification	60
2.5.5	Evaluation	61
2.6	Epoxide – a ring opening study	63
2.7	The mechanism of activation of CO ₂	64
2.8	Effect of water	64
2.9	Reusability and re-characterization of catalyst	64
CHAPTER 3 – CATALYST CHARACTERIZATION		65

3.1	Characterization of MCM-41, Cl-MCM-41 and MCM-41-Imi	65
3.1.1	FT-IR analysis	65
3.1.2	Nitrogen adsorption - desorption analysis	67
3.1.3	²⁹ Si CP/MAS NMR spectroscopic analysis	73
3.1.4	¹³ C CP/MAS NMR spectroscopic analysis	75
3.1.5	SEM/EDS analysis	77
3.1.6	TEM	80
3.1.7	XRD analysis	82
3.1.8	CHN analysis	87
3.1.9	TG-DTG analysis	88
3.2	Characterization of MCM-41 Imi/X (X=Cl, Br, I)	91
3.2.1	FT-IR analysis	91
3.2.2	Nitrogen adsorption - desorption analysis	94
3.2.3	²⁹ Si CP/MAS NMR spectroscopic analysis	99
3.2.4	¹³ C CP/MAS NMR spectroscopic analysis	100
3.2.5	SEM/EDS	102
3.2.6	TEM analysis	105
3.2.7	IC analysis	107
3.2.8	Redox titration analysis	107
3.2.9	XRD analysis	108
3.2.10	CHN analysis	112
3.2.11	TG-DTG analysis	113
	CHAPTER 4 – THE CYCLOADDITION OF CO₂ WITH EPOXIDE	117
4.1	General introduction	117
4.2	Cycloaddition of CO ₂ with styrene oxide	118

4.2.1	Introduction	118
4.2.2	Effect of control catalyst	119
4.2.3	Effect of reaction temperature	121
4.2.4	Effect of initial pressure	122
4.2.5	Effect of catalyst amount	124
4.2.6	Effect of reaction time	125
4.2.7	Effect of solvent	126
4.2.8	Product identification	130
	4.2.8.1 FT-IR analysis	130
	4.2.8.2 GC-MS analysis	131
	4.2.8.3 ¹ H NMR analysis	133
4.3	Cycloaddition of CO ₂ with epichlorohydrin	137
	4.3.1 Introduction	137
	4.3.2 Effect of temperature	138
	4.3.3 Effect of initial pressure	139
	4.3.4 Effect of catalyst mass	140
	4.3.5 Effect of time	141
4.4	Cycloaddition of CO ₂ with glycidol	143
	4.4.1 Introduction	143
	4.4.2 Effect of temperature	144
	4.4.3 Effect of initial pressure	146
	4.4.4 Effect of catalyst mass	147
	4.4.5 Effect of time	148
4.5	Cycloaddition of CO ₂ with allyl glycidyl ether	149
	4.5.1 Introduction	149
	4.5.2 Effect of temperature	150

4.5.3	Effect of initial pressure	151
4.5.4	Effect of catalyst mass	152
4.5.5	Effect of time	153
4.6	Cycloaddition of CO ₂ with phenyl glycidyl ether	155
4.6.1	Introduction	155
4.6.2	Effect of temperature	155
4.6.3	Effect of initial pressure	156
4.6.4	Effect of catalyst mass	157
4.6.5	Effect of time	159
4.7	Cycloaddition of CO ₂ with 1,2-epoxyhexane	160
4.7.1	Introduction	160
4.7.2	Effect of temperature	161
4.7.3	Effect of initial pressure	162
4.7.4	Effect of catalyst mass	162
4.7.5	Effect of time	163
4.8	The overall reactivity of MCM-41-Imi/Br for the cycloaddition of the epoxides	164
4.9	Effect of different catalysts	168
4.10	Reusability of MCM-41-Imi/Br	171
4.11	Characterization of used catalyst	172
4.11.1	TEM analysis	172
4.11.2	Ion chromatography analysis	173
4.11.3	XRD analysis	173
CHAPTER 5 – THE ELUCIDATION OF REACTION MECHANISM USING MCM-41-IMI/BR AND MCM-41-IMI CATALYSTS		175

5.1	Ring opening of epoxide using MCM-41-Imi/Br	175
5.2	Ring opening of epoxide using MCM-41-Imi	177
5.3	Effect of water	180
5.4	Activation of CO ₂	180
5.5	Reaction mechanism (CO ₂ activated at tertiary amine)	183
5.6	Reaction mechanism (CO ₂ activated at quaternary ammonium ion)	184
CHAPTER 6 – CONCLUSION AND FUTURE OUTLOOK		187
6.1	Conclusion	187
6.2	Future outlook	191
REFERENCES		193
APPENDICES		209
LIST OF PUBLICATIONS AND PRESENTATIONS IN CONFERENCES		237

LIST OF TABLES

		Page
Table 1.1	Catalytic activity studies of cycloaddition of CO ₂ to styrene oxide using various homogeneous and heterogeneous catalysts.	11
Table 2.1	Chemicals used for the catalyst preparation.	44
Table 2.2	Chemicals used for the physico-chemical characterizations.	45
Table 2.3	Chemicals used for the product identification and for the catalytic reaction.	45
Table 2.4	Final molar composition of the solution.	47
Table 2.5	The GC analysis conditions for various epoxides.	60
Table 3.1	The textural properties of the prepared materials.	71
Table 3.2	CHN elemental analysis of the catalysts.	87
Table 3.3	The textural properties of the prepared materials.	98
Table 3.4	CHN elemental analysis of the catalysts.	112
Table 4.1	Reaction profile in the cycloaddition of SO with CO ₂ over various catalysts.	119
Table 4.2	The effect of solvents on the cycloaddition reaction of CO ₂ with styrene oxide.	127
Table 4.3	The synthesis of styrene carbonate from cycloaddition of CO ₂ under solvent free conditions. A summary of reaction parameters.	128
Table 4.4	The chemical shifts, splitting pattern and <i>J</i> coupling of protons in styrene carbonate.	133
Table 4.5	Influence of the initial CO ₂ pressure on the conversion, selectivity, yield and TOF.	140
Table 4.6	Effect of catalyst mass in the cycloaddition of EPCH with CO ₂ over MCM-41-Imi/Br.	140

Table 4.7	Influence of pressure on conversion, selectivity, yield and TOF of cycloaddition of glycidol and CO ₂ .	146
Table 4.8	Influence of the initial CO ₂ pressure on the conversion, selectivity, yield and TOF in the cycloaddition of AGE and CO ₂ .	152
Table 4.9	Influence of initial CO ₂ pressure on the cycloaddition of EH and CO ₂ .	162
Table 4.10	The suitable reaction condition for cycloaddition of CO ₂ with epoxides using MCM-41-Imi/Br.	165
Table 4.11	Influence of the catalyst amount on the yield of the cycloaddition of CO ₂ with epoxides.	167
Table 4.12	The effect of different anion on the cycloaddition reaction of CO ₂ with various epoxides. The preferential reaction conditions were used as MCM-41-Imi/Br catalyst.	169

LIST OF FIGURES

		Page
Figure 1.1	The Keeling Curve: Atmospheric CO ₂ concentration for the period of 1958 to 2012 (McGee, 2013).	2
Figure 1.2	A summary of organic transformations using CO ₂ .	4
Figure 1.3	A heap of rice husk in a local rice mill.	27
Figure 1.4	The structures of mesoporous M41S materials: (a) MCM-41 (2D hexagonal, space group p6mm), (b) MCM-48 (cubic, space group Ia3d), and (c) MCM-50 (lamellar, space group p2) (Gibson, 2014).	31
Figure 1.5	TEM micrograph of MCM-41. The mesopores are arranged in a honeycomb-like structure, separated by thin, amorphous silica pore walls (black) (He et al., 2013).	33
Figure 2.1	The schematic diagram of (a) high pressure laboratory autoclave and (b) top view of head assembly of autoclave. This print is the property and copyright of AMAR EQUIPMENTS PVT. LTD. MUMBAI-400 070.	58
Figure 3.1	The FT-IR spectra of MCM-41 (a) after calcination at 600 °C for 6 h and (b) before calcination.	65
Figure 3.2	The FT-IR spectra of Cl-MCM-41 and MCM-41-Imi. The magnified graph shows the FT-IR spectra in the region of 1700-1500 cm ⁻¹ .	67
Figure 3.3	N ₂ adsorption-desorption isotherm of MCM-41, Cl-MCM-41 and MCM-41-Imi.	68
Figure 3.4	The PSD curve for MCM-41, Cl-MCM-41 and MCM-41-Imi.	70
Figure 3.5	Hexagonal arrangement of the mesoporous structure of MCM-41, Cl-MCM-41 and MCM-41-Imi showing the unit cell parameter (a_0), wall thickness (W_t), interplanar distance (d_{100}) and pore size diameter (D_p) (Coriolano et al., 2013).	72
Figure 3.6	The ²⁹ Si CP/MAS NMR spectrum of (a) MCM-41, (b) Cl-MCM-41 and (c) MCM-41-Imi.	74
Figure 3.7	The ¹³ C CP/MAS NMR spectra of (a) Cl-MCM-41 and (b) MCM-41-Imi.	76

Figure 3.8	SEM micrographs of (a) MCM-41 at x 15 k, (b) MCM-41 at x 20 k, (c) Cl-MCM-41 at x 3 k and (d) MCM-41-Imi at x 9 k.	77
Figure 3.9	EDS profile of Cl-MCM-41. Inset shows the SEM image of Cl-MCM-41.	79
Figure 3.10	EDS profile of MCM-41-Imi. Inset shows the SEM micrograph of MCM-41-Imi.	80
Figure 3.11	The TEM micrographs of (a) MCM-41 at x 240 k, (b) MCM-41 at x 450 k (c) Cl-MCM-41 at x 450 k and (d) MCM-41-Imi at x 550 k.	81
Figure 3.12	(a) Low angle X-ray diffraction pattern and (b) high angle diffraction pattern of MCM-41.	83
Figure 3.13	(a) Low angle X-ray diffraction pattern of Cl-MCM-41 and (b) MCM-41-Imi.	85
Figure 3.14	(a) High angle X-ray diffraction pattern of Cl-MCM-41 and (b) MCM-41-Imi.	86
Figure 3.15	TG-DTG curves of (a) MCM-41 (before calcination) and (b) MCM-41 (after calcination).	89
Figure 3.16	TG-DTG curves of (a) Cl-MCM-41 and (b) MCM-41-Imi.	90
Figure 3.17	The FT-IR spectra of MCM-41-Imi/Cl, MCM-41-Imi/Br and MCM-41-Imi/I.	92
Figure 3.18	The expansion of the FT-IR spectra of MCM-41 and MCM-41-Imi/X (X= Cl, Br and I) in the region of 1700-1500 cm^{-1} . The band at 1619 cm^{-1} showing the presence of C=N vibration in the conjugated imidazole.	93
Figure 3.19	The expansion of the FT-IR spectra of MCM-41 and MCM-41-Imi/X (X= Cl, Br and I) in the region of 3000-3600 cm^{-1} . The band at 3414 cm^{-1} showing the ionic nature of the N^+X^- (Udayakumar et al., 2009a).	94
Figure 3.20	The N_2 adsorption-desorption isotherms of MCM-41-Imi/Cl, MCM-41-Imi/Br and MCM-41-Imi/I.	95
Figure 3.21	PSD curves of (a) MCM-41-Imi/Cl, (b) MCM-41- Imi/Br and (c) MCM-41-Imi/I.	97
Figure 3.22	The ^{29}Si CP/MAS NMR spectrum of (a) MCM-41-Imi/Cl, (b) MCM-41-Imi/Br and (c) MCM-41-Imi/I.	99

Figure 3.23	The ¹³ C CP/MAS NMR spectrum of (a) MCM-41-Imi/Cl (b) MCM-41-Imi/Br and (c) MCM-41-Imi/I.	101
Figure 3.24	SEM micrographs of (a) MCM-41-Imi/Cl at x 10 k, (b) MCM-41-Imi/Br at x 9 k, and (c) MCM-41-Imi/I at 13 k.	102
Figure 3.25	SEM micrograph and EDS profile of MCM-41-Imi/Cl.	103
Figure 3.26	SEM micrograph and EDS profile of MCM-41-Imi/Br.	104
Figure 3.27	SEM micrograph and EDS profile of MCM-41-Imi/I.	105
Figure 3.28	The TEM micrographs of (a) MCM-41-Imi/Cl at x 550 k, (b) MCM-41-Imi/Br at x 260 k, and (c) MCM-41-Imi/I at 450 k.	106
Figure 3.29	The low angle XRD pattern of (a) MCM-41-Imi/Cl, (b) MCM 41-Imi/Br, (c) MCM-41-Imi/I.	110
Figure 3.30	The high angle XRD pattern of (a) MCM-41-Imi/Cl, (b) MCM-41-Imi/Br, (c) MCM-41-Imi/I.	112
Figure 3.31	TG-DTG curves of (a) MCM-41-Imi/Cl, (b) MCM-41-Imi/Br and (c) MCM-41-Imi/I.	115
Figure 4.1	The effect of temperature on the cycloaddition of CO ₂ with SO catalysed by MCM-41-Imi/Br. The percentage conversion and selectivity to styrene carbonate at different reaction temperature. Reaction conditions: amount of SO = 3.5 mL (30 mmol), initial CO ₂ pressure = 60 bar, catalyst mass = 300 mg, acetonitrile = 50 mL and time = 8 h.	121
Figure 4.2	The effect of initial pressure on the cycloaddition activity. Reaction conditions: amount of SO = 3.5 mL (30 mmol), temperature = 140 °C, MCM-41- Imi/Br = 300 mg, acetonitrile = 50 mL and time = 8 h.	123
Figure 4.3	The effect of catalyst mass on the cycloaddition of CO ₂ with SO catalysed by MCM-41-Imi/Br. Reaction conditions: Catalyst used: MCM-41-Imi/Br, amount of SO = 3.5 mL (30 mmol), temperature = 140 °C, initial CO ₂ pressure = 40 bar, acetonitrile = 50 mL and time = 8 h.	124
Figure 4.4	The effect of reaction time on the cycloaddition of CO ₂ with SO Reaction conditions: amount of SO = 3.5 mL (30 mmol), temperature = 140 °C, initial CO ₂ pressure = 40 bar, MCM-41-Imi/Br = 300 mg and acetonitrile = 50 mL.	126

Figure 4.5	The FT-IR spectra of (a) styrene oxide and (b) styrene carbonate.	131
Figure 4.6	(a) The chromatogram of the SC and (b) The mass spectrum from the GC-MS analysis.	132
Figure 4.7	The ^1H NMR spectrum of styrene carbonate.	134
Figure 4.8	The magnified ^1H NMR spectrum of styrene carbonate.	135
Figure 4.9	Catalytic performance of MCM-41-Imi/Br as a function of temperature in the synthesis of chloropropene carbonate from CO_2 and EPCH. Reaction conditions: amount of epichlorohydrin = 2.3 mL (30 mmol), initial CO_2 pressure = 30 bar, catalyst mass = 300 mg, and time = 4 h.	138
Figure 4.10	The effect of reaction time on the cycloaddition of CO_2 with EPCH catalyzed by MCM-41-Imi/Br. Reaction conditions: amount of EPCH = 2.3 mL (30 mmol), temperature = 90 °C, initial CO_2 pressure = 25 bar and catalyst mass = 300 mg.	142
Figure 4.11	Catalytic performance of MCM-41-Imi/Br as a function of temperature in the synthesis of GC from CO_2 and GOH. Reaction conditions: amount of GOH = 2.0 mL (30 mmol), initial CO_2 pressure = 20 bar, catalyst mass = 300 mg and time = 4 h.	145
Figure 4.12	The activity profile over different catalyst masses. Reaction conditions: amount of GOH = 2.0 mL (30 mmol), catalyst used = MCM-41-Imi/Br, temperature = 90 °C, initial CO_2 pressure = 20 bar and time = 4 h.	147
Figure 4.13	Curve showing the effect of reaction time on the cycloaddition of CO_2 with GOH catalysed by MCM-41-Imi/Br. Reaction conditions: amount of GOH = 2.0 mL (30 mmol), temperature = 90 °C, initial CO_2 pressure = 20 bar and catalyst mass = 300 mg.	148
Figure 4.14	Catalytic performance of MCM-41-Imi/Br as a function of temperature in the synthesis of AGC from CO_2 and AGE. Reaction conditions: amount of AGE = 3.5 mL (30 mmol), initial CO_2 pressure = 60 bar, catalyst mass = 300 mg and time = 6 h.	151
Figure 4.15	The effect of catalyst mass on the cycloaddition of CO_2 with AGE catalyzed by MCM-41-Imi/Br. Reaction conditions: amount of AGE = 3.5 mL (30 mmol), temperature = 120 °C, initial CO_2 pressure = 60 bar and time = 6 h.	153

Figure 4.16	The effect of the reaction time on the cycloaddition of CO ₂ with AGE catalyzed by MCM-41-Imi/Br. Reaction conditions: amount of AGE = 3.5 mL (30 mmol), temperature = 120 °C, initial CO ₂ pressure = 60 bar and catalyst mass = 300 mg.	154
Figure 4.17	Catalytic performance of MCM-41-Imi/Br as a function of temperature in the synthesis of PGC from CO ₂ and PGE. Reaction conditions: amount of PGE = 4.0 mL (30 mmol), initial CO ₂ pressure = 40 bar, catalyst mass = 400 mg and time = 6 h.	156
Figure 4.18	The influence of initial CO ₂ pressure in the synthesis of PGC from CO ₂ and PGE. Reaction conditions: amount of PGE = 4.0 mL (30 mmol), temperature = 100 °C, catalyst mass = 400 mg and time = 6 h.	157
Figure 4.19	Catalytic performance of MCM-41-Imi/Br as a function of catalyst mass in the synthesis of PGC from CO ₂ and PGE. Reaction conditions: amount of PGE = 4.0 mL (30 mmol), temperature = 100 °C, initial CO ₂ pressure = 20 bar and time = 6 h.	158
Figure 4.20	Catalytic performance of MCM-41-Imi/Br as a function of reaction time in the synthesis of PGC from CO ₂ and PGE. Reaction conditions: amount of PGE = 4.0 mL (30 mmol), temperature = 100 °C, initial CO ₂ pressure = 20 bar and catalyst mass = 300 mg.	159
Figure 4.21	Catalytic performance of MCM-41-Imi/Br as a function of temperature in the synthesis of 4-BD from CO ₂ and EH. Reaction conditions: amount of EH = 3.6 mL (30 mmol), initial CO ₂ pressure = 30 bar, catalyst mass = 300 mg and time = 4 h.	161
Figure 4.22	Catalytic performance of MCM-41-Imi/Br as a function of catalyst mass in the synthesis of 4-BD from CO ₂ and EH. Reaction conditions: amount of EH = 3.6 mL (30 mmol), temperature = 100 °C, initial CO ₂ pressure = 20 bar and time = 4 h.	163
Figure 4.23	Catalytic performance of MCM-41-Imi/Br as a function of reaction time in the synthesis of 4-BD from CO ₂ and, EH. Reaction conditions: amount of EH = 3.6 mL (30 mmol), temperature = 100 °C, initial CO ₂ pressure = 20 bar and catalyst mass = 300 mg.	164

Figure 4.24	MCM-41-Imi/Br reusability analysis in the CO ₂ cycloaddition with SO. Reaction conditions: time = 4 h, temperature = 140 °C, initial CO ₂ pressure = 40 bar, catalyst mass = 300 mg, SO = 3.5 mL (30 mmol), solvent = nil.	172
Figure 4.25	The TEM images of used MCM-41-Imi/Br. (a) The view direction is along the pore axis. The long range of highly ordered hexagonal pores could be clearly seen at x 400 k and (b) The curved pores originate from longitudinal and transverse disclination shown at 240 k.	173
Figure 4.26	The low-angle XRD pattern of used MCM-41-Imi/Br.	174
Figure 5.1	(a) The GC-MS spectrum of the intermediate (2-bromo-1-phenylethanol and by-product (styrene glycol) from the reaction of styrene oxide with MCM-41-Imi/Br, the mass spectral data of (b) 2-bromo-1-phenylethanol and (c) styrene glycol.	176
Figure 5.2	The GC-MS spectrum of the by-products (styrene glycol) and (2-phenethoxy-1-phenylethanol or 2-phenethoxy-2-phenylethanol) from the reaction of styrene oxide with MCM-41-Imi, the mass spectral data of (b) styrene glycol and (c) 2-phenylethoxy-1-phenylethanol or 2-phenylethoxy-2-phenylethanol.	179
Figure 5.3	The FT-IR spectra of the MCM-41-Imi/Br. (i) fresh catalyst (ii) after the first reaction; (iii) adsorption of catalyst with CO ₂ .	181

LIST OF SCHEMES

		Page
Scheme 1.1	Synthesis of organic carbonate through conventional method.	6
Scheme 1.2	Cycloaddition of CO ₂ to epoxide forming cyclic carbonate.	6
Scheme 1.3	Role of DMF in the cycloaddition of epoxides (Aresta et al., 2003).	17
Scheme 1.4	The assumed reaction mechanism for the cycloaddition of epoxide with CO ₂ catalyzed by HBetX (Zhou et al., 2008).	21
Scheme 1.5	The carbon and oxygen atoms act as Lewis acid and Lewis base respectively. Both are potential activation sites.	23
Scheme 1.6	Hypothesized MTBD-promoted CO ₂ activation (Barbarini et al., 2003).	24
Scheme 1.7	Different types of coordination modes of CO ₂ (Srivastava et al., 2006a).	25
Scheme 1.8	CO ₂ activation through primary, secondary and tertiary amines (Srivastava et al., 2006a).	26
Scheme 1.9	The formation of MCM-41 using TEOS as a silica precursor with a structure directing agent (SDA) (Hoffmann et al., 2006).	34
Scheme 1.10	Grafting method for organic modification of mesoporous pure silica phase with terminal organosilanes. R = organic functional group (Hoffmann et al., 2006, Rath et al., 2014).	35
Scheme 1.11	Co-condensation method for the modification of mesoporous pure silica phase. R = organic functional group (Hoffmann et al., 2006).	37
Scheme 1.12	General synthetic pathway to PMOs that are constructed from bisilylated organic bridging units. R= organic bridge (Hoffmann et al., 2006).	39
Scheme 2.1	The reaction sequence and the possible structure for MCM-41-Imi/Br.	49
Scheme 2.2	The postulated structures of (a) MCM-41-Imi/Cl and (b) MCM-41-Imi/I, showing the bonding connections of the organic ligands.	50

Scheme 2.3	Cycloaddition of epoxide (A) to CO ₂ (B) forming cyclic carbonate (C) and by-product (D). R is alkyl or aryl group.	61
Scheme 5.1	Reaction of MCM-41-Imi/Br with epoxide in the absence of CO ₂ : Most likely position for a nucleophilic attack of the ring and possible role of water molecule in the formation of intermediate and/or by-product.	175
Scheme 5.2	Reaction of MCM-41-Imi with epoxide in the absence of CO ₂ : The role of water molecule in the formation of by-product.	178
Scheme 5.3	The proposed CO ₂ activation via (a) tertiary amine forming activated CO ₂ carbamate anion and (b) quarternary ammonium ion of MCM-41-Imi/Br.	182
Scheme 5.4	The mechanism of formation of intermediate and cyclic carbonate in the presence of CO ₂ . The CO ₂ is activated by tertiary amine.	183
Scheme 5.5	The proposed reaction mechanism for cycloaddition of epoxide and CO ₂ catalyzed MCM-41-Imi/Br: The simultaneous activation of epoxide and CO ₂ on a catalyst.	185
Scheme 6.1	The synthesis of homogeneous Imi-Br with the structure of MCM-41-Imi/Br.	190

LIST OF APPENDICES

	Page
Appendix A Catalyst characterization-EDS analysis	209
Figure A1 EDS area analysis data of Cl-MCM-41.	210
Figure A2 EDS spot analysis data of Cl-MCM-41.	211
Figure A3 EDS area analysis data of MCM-41-Imi.	212
Figure A4 EDS area analysis data of MCM-41-Imi.	213
Figure A5 EDS area analysis data of MCM-41-Imi/Cl.	214
Figure A6 EDS spot analysis data of MCM-41-Imi/Cl.	215
Figure A7 EDS area analysis data of MCM-41-Imi/Br.	216
Figure A8 EDS spot analysis data of MCM-41-Imi/Br.	217
Figure A9 EDS spot analysis data of MCM-41-Imi/I.	218
Figure A10 EDS spot analysis data of MCM-41-Imi/I.	219
Appendix B Ion chromatogram for the MCM-41-Imi/Cl, MCM-41-Imi/Br and reused MCM-41-Imi/Br	220
Figure B1 Ion chromatogram of MCM-41-Imi/Cl.	221
Figure B2 Ion chromatogram of MCM-41-Imi/Br.	222
Figure B3 Ion chromatogram of used MCM-41-Imi/Br.	223
Appendix C Example of TOF calculation	224
Appendix D GC-MS analysis for the cycloaddition of CO₂ to epoxides	226
Figure D1 GC-MS analysis data for the cycloaddition of epichlorohydrin (EPCH) with CO ₂ over MCM-41-Imi/Br at 0 h.	227
Figure D2 GC-MS analysis data for the cycloaddition of epichlorohydrin (EPCH) with CO ₂ over MCM-41-Imi/Br at 4 h.	228

Figure D3	GC-MS analysis data for the cycloaddition of glycidol (GOH) with CO ₂ over MCM-41-Imi/Br at 0 h.	229
Figure D4	GC-MS analysis data for the cycloaddition of glycidol (GOH) with CO ₂ over MCM-41-Imi/Br at 4 h.	230
Figure D5	GC-MS analysis data for the cycloaddition of allyl glycidyl ether (AGE) with CO ₂ over MCM-41-Imi/Br at 0 h.	231
Figure D6	GC-MS analysis data for the cycloaddition of allyl glycidyl ether (AGE) with CO ₂ over MCM-41-Imi/Br at 6 h.	232
Figure D7	GC-MS analysis data for the cycloaddition of phenyl glycidyl ether (PGE) with CO ₂ over MCM-41-Imi/Br at 0 h.	233
Figure D8	GC-MS analysis data for the cycloaddition of phenyl glycidyl ether (PGE) with CO ₂ over MCM-41-Imi/Br at 3 h.	234
Figure D9	GC-MS analysis data for the cycloaddition of 1,2-epoxyhexane (EH) with CO ₂ over MCM-41-Imi/Br at 0 h.	235
Figure D10	GC-MS analysis data for the cycloaddition of 1,2-epoxyhexane (EH) with CO ₂ over MCM-41-Imi/Br at 3 h.	236

LIST OF SYMBOLS AND ABBREVIATIONS

1,3-DCP	1,3-dichloropropan-2-ol
^{13}C CP/MAS NMR	Carbon-13 Cross Polarisation/Magic Angle Spinning Nuclear Magnetic Resonance
^1H NMR	Proton Nuclear Magnetic Resonance
^{29}Si CP/MAS NMR	Silicon -29 Cross Polarisation/Magic Angle Spinning Nuclear Magnetic Resonance
3-AP	3-(allyloxy)propane-1,2-diol
3-BP	3-bromo-1,2-propanediol
3-CP	3-chloropropane-1,2-diol
3-MMP	3-methoxypropanoate
4-BD	4-butyl-1-3-dioxolan-2-one
a_0	Lattice value or hexagonal unit cell parameter
Ade	Adenine
AGC	Allyl Glycidyl Carbonate
AGE	Allyl Glycidyl Ether
BET	Barret-Joyner-Halenda
BJH	Brunauer-Emmett-Teller
CC	Chloropropene Carbonate
CHN	Carbon, Hydrogen, Nitrogen
CNT	Carbon NanoTubes
CPTES	3-(chloropropyl)triethoxysilane
CTAB	Cetyltrimethylammonium bromide
CTAC	Cetyltrimethylammonium chloride

d_{100}	Diffraction plane-100
DMA	Dimethyl acetamide
DMF	<i>N,N</i> -dimethylformamide
DMSO	Dimethyl sulfoxide
EDS	Energy Dispersive X-ray spectroscopy
EH	1,2-epoxyhexane
EPCH	Epichlorohydrin
FT-IR	Fourier Transform Infra-Red spectrometry
GC	Gas chromatograph
GC	Glycerol Carbonate
GC-MS	Gas chromatograph interfaced to a mass spectrometer
Gly	Glycerol
GOH	Glycidol
Gua	Guanine
hkl	Miller indices
IC	Ion Chromatograph
IL	Ionic-Liquid
Imi	Imidazole
IUPAC	International Union of Pure and Applied Chemistry
M	Molar amount of grafted organic phase
M^{\dagger}	The molecular ion
m/z	The mass of ion divided by its charge
MCM	Mobil Crystalline Material
MWCNT	Multi Wall Carbon Nanotubes

<i>N</i>	Surface coverage
<i>n</i>	Number of carbon atoms per organic molecule
NMR	Nuclear Magnetic Resonance
P/P_0	Relative pressure
P_c	Percentage of carbon
PC	Propylene carbonate
PGC	Phenyl Glycidyl Carbonate
PGE	Phenyl Glycidyl Ether
PMO	Periodic Mesoporous Organosilane
PO	Propylene Oxide
POM	Partial Oxidation of Methanol
PSD	Pore Size Distribution
P_w	Weight Percentage (amount of organic ligand grafted)
R	Alkyl or aryl group
RH	Rice Husk
RHA	Rice Husk Ash
rpm	rotations per minute
RT	Retention Time
S	Specific surface area
SBA	Santa Barbara Amorphous
sc	Super critical
SC	Styrene Carbonate
SDA	Structure Directing Agent
SEM	Scanning Electron Microscope

SG	Styrene Glycol
SO	Styrene Oxide
TEM	Transmission Electron Microscope
TEOS	Tetraethylorthosilicate
TG-DTG	Thermogravimetry- Derivative Thermogram
TOF	Turnover frequency
TON	Turnover number
USY	Ultrastable Y-type Zeolite
W_t	wall thickness
wt. %	weight percentage
XRD	X-ray Diffraction
ZIF-8	Zeolitic imidazolate frameworks
ZSM-5	Zeolite Socony Mobil-5

**SINTESIS, PENCIRIAN DAN AKTIVITI PEMANGKINAN MCM-41
IMIDAZOLIUM HALIDA MANGKIN BAGI TINDAK BALAS
ANTARA EPOKSIDA DAN KARBON DIOKSIDA**

ABSTRAK

Penetapan kimia karbon dioksida (CO₂) telah mendapat perhatian yang semakin meningkat sebagai sumber karbon yang berpotensi dalam proses kimia perindustrian berikutan kebimbangan yang semakin meningkat daripada kesan rumah hijau. Salah satu cara yang paling menjanjikan untuk penggunaan berharga CO₂ adalah melalui sintesis karbonat siklik. Dalam karya ini, sintesis karbonat siklik dan kajian mekanistik tindak balas penambahan siklik antara epoksida dan CO₂ menggunakan mangkin MCM-41-Imidazolium halida telah diteroka. MCM-41 telah disediakan daripada abu sekam padi (RHA) dengan menggunakan cetiltrimetilammonium bromida (CTAB) melalui kaedah sol-gel. MCM-41 telah dimodifikasikan dengan imidazol menggunakan 3-(kloropropil)trietoksisilana (CPTES) diikuti oleh pengalkilan dengan 1,2-dihaloethana. Pencirian spektroskopi membuktikan pencantuman ligan organik pada rangka silika. Tindak balas penambahan siklik telah dijalankan menggunakan autoklaf makmal tekanan tinggi di bawah keadaan tanpa pelarut. Hasil karbonat siklik masing-masing menggunakan MCM-41-Imi/Br ialah: 98.8 % bagi stirena oksida, 97.0 % bagi epiklorohidrina, 98.3 % bagi glisidol, 97.5 % bagi alil glisidil eter, 96.7 % bagi fenil glisidil eter dan 100 % untuk 1,2-epoksiheksana. Untuk semua mangkin yang lain, analisis produk menunjukkan pembentukan karbonat siklik masing-masing pada hasil yang tinggi melebihi 97.0%. Pembukaan gelang stirena oksida dan eksperimen pengaktifan CO₂ telah dijalankan. Pembukaan gelang stirena oksida berlaku pada atom

karbon yang kurang dihalang (β -karbon) melalui serangan nukleofilik ion bromida. Analisis GC-MS menunjukkan kehadiran dua produk yaitu 2-bromo-1-feniletanol (produk perantaraan) dan stirena glikol sebagai hasil sampingan. Molekul CO_2 diaktifkan oleh kumpulan beralkali nitrogen daripada imidazol yang telah disahkan oleh analisis FT-IR. Dua mekanisma yang munasabah telah dicadangkan bagi tindak balas pemangkinan. Pembukaan gelang epoksida yang berlaku melalui serangan nukleofilik oleh ion halida membentuk spesies haloalkoksi. Pada masa yang sama, CO_2 diaktifkan oleh amina tersier melalui ikatan koordinat hidrogen berasid daripada imidazol membentuk ikatan hidrogen dengan salah satu daripada oksigen karbon dioksida. Begitu juga, CO_2 juga boleh diaktifkan melalui oksigen daripada karbon dioksida dengan cara ikatan koordinat ion ammonium kuarternari daripada mangkin. Ion ammonium kuarternari atau amina tersier dan anion halida menunjukkan kesan sinergi untuk mempromosikan tindak balas, yang bertanggungjawab untuk aktiviti pemangkinan yang tinggi dan berselektif.

SYNTHESIS, CHARACTERIZATION AND CATALYTIC ACTIVITY OF MCM-41 IMIDAZOLIUM HALIDE CATALYSTS FOR THE REACTION BETWEEN EPOXIDES AND CARBON DIOXIDE

ABSTRACT

The chemical fixation of carbon dioxide (CO₂) has received increasing attention as a potential carbon source in industrial chemical processes due to the growing concern of the greenhouse effect. One of the most promising ways for valuable utilization of CO₂ is the synthesis of cyclic carbonates. In this work, the synthesis of cyclic carbonates and mechanistic study of cycloaddition reaction between epoxides and CO₂ using MCM-41-Imidazolium halide catalysts were explored. MCM-41 was prepared from rice husk ash (RHA) using cetyltrimethylammonium bromide (CTAB) via sol-gel method. MCM-41 was functionalized with imidazole using 3-(chloropropyl)triethoxysilane (CPTES) followed by alkylation with 1,2-dihaloethane. Spectroscopic characterization confirmed the successful immobilization of organic ligand on the silica framework. The cycloaddition reactions were carried out in high pressure laboratory autoclave under solvent less condition. The yields of the respective cyclic carbonates using MCM-41-Imi/Br were: 98.8 % for styrene oxide, 97.0 % for epichlorohydrin, 98.3 % for glycidol, 97.5 % for allyl glycidyl ether, 96.7 % for phenyl glycidyl ether and 100 % for 1,2-epoxyhexane. For all the other catalysts, the product analysis revealed the formation of the respective cyclic carbonates at high yield of more than 97.0 %. The ring opening of styrene oxide and the activation of CO₂ experiments were carried out. The ring opening of styrene oxide occurred at the less hindered carbon atom (β -carbon) via the nucleophilic attack of the bromide ion. The GC-MS analysis

showed the presence of two products which corresponds to 2-bromo-1-phenylethanol (intermediate product) and styrene glycol as a by-product. CO₂ molecules are activated at the basic nitrogen group of imidazole which was confirmed by FT-IR analysis. Two plausible reaction mechanisms were proposed for the catalytic reaction. The ring opening of the epoxide was shown to take place by means of a nucleophilic attack by the halide ion forming the haloalkoxy species. Simultaneously, the CO₂ was activated by the tertiary amine through the coordinate bond of the acidic hydrogen from the imidazole forming a hydrogen bond with one of the oxygen of the carbon dioxide. Similarly, the CO₂ can also be activated through the oxygen of the CO₂ by way of a coordinate bond to the quaternary ammonium ion of the catalyst. The quaternary ammonium ion or tertiary amine and the halide anion are shown to exhibit a synergistic effect to promote the reaction, which is responsible for the high catalytic activity and selectivity.

CHAPTER 1

INTRODUCTION

1.1 Global warming

Naturally, the presence of carbon dioxide (CO₂) in the atmosphere is to help in the photosynthesis of plants for their food. Although this gas plays a pivotal role for all the living things in the world, it is also the main constituent among the greenhouse gases and it circulates in the environment through a carbon cycle (Srivastava et al., 2005a). About 32 % of CO₂ is produced due to hydrocarbon combustion and gasification which are released into the atmosphere. The use of fossil fuel in transportation releases ~30 % of the total CO₂. Natural phenomena such as volcanic eruption and decay of plants and animals too release CO₂ into the atmosphere.

As a consequence, the CO₂ concentration increases in the atmosphere and results in climate change due to the greenhouse effect (Alvaro et al., 2005). Figure 1.1 shows the changes in the global atmospheric CO₂ concentration for 55 years since 1958 which was based on continuous measurement recorded at the Mauna Loa Observatory in Hawaii. The concentration of atmospheric CO₂ was 399.89 ppm till May 2013, and it is estimated to reach 550 ppm by the year 2020 (McGee, 2013). The continuous rise in atmospheric CO₂ concentration resulted in global warming leading to serious environmental issues including melting of glacier, drought, flood, rising of sea level and damage of habitat and living species.

Increasing concern in global climate changes has necessitated various forums, debates and international programs to brainstorm ways of reducing the rate of emission of CO₂ into the atmosphere. In recent years, various utilization of this naturally abundant CO₂ has gained considerable attention as part of an effort to reduce the concentration of CO₂ in the atmosphere.

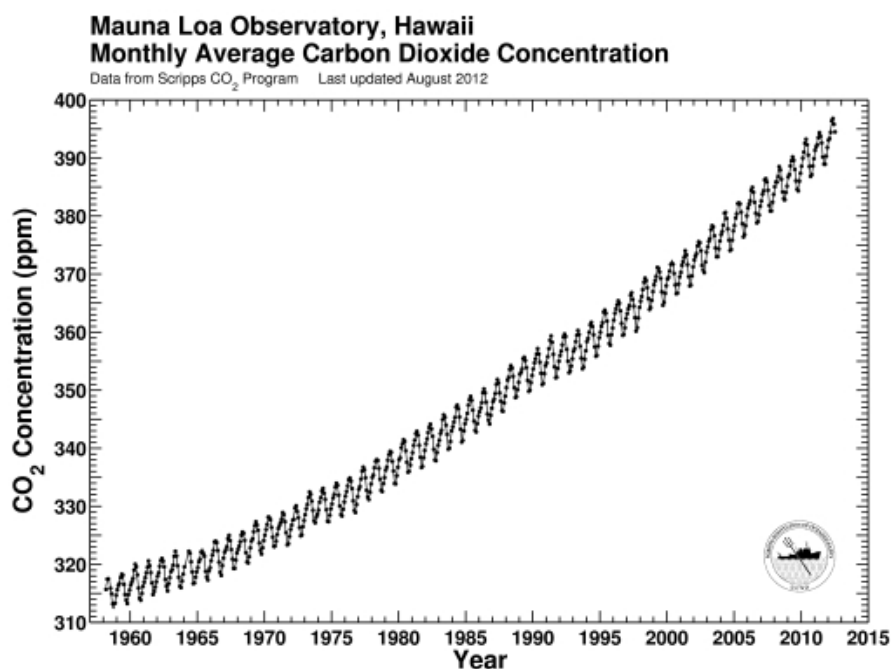


Figure 1.1: The Keeling Curve: Atmospheric CO₂ concentration for the period of 1958 to 2012 (McGee, 2013).

1.2 Carbon dioxide

Carbon dioxide is a colourless and odourless gas. It is a linear molecule with double bonds between the carbon and oxygen atoms (O=C=O). The central carbon atom is sp hybridized and the C–O bond length is 1.16 Å. This bond length is shorter than a C=O double bond involving a sp² hybridized carbon atom.

Carbon dioxide is recognized as a non-flammable, non-toxic (Liu et al., 2014), inexpensive reagent and environmentally benign molecule (Barbarini et al., 2003). It is a safe, renewable carbon source (Zhou et al., 2008) and thermodynamically stable compound (Alvaro et al., 2004). It is kinetically inert (Dai et al., 2010, Alvaro et al., 2004), and is used as C1 building block in organic synthesis (Dai et al., 2010). More importantly it can be substituted in chemical reactions for carbonyl dichloride known as phosgene (COCl_2), carbon monoxide (CO) and isocyanides (R-NCO) as these compounds are poisonous and toxic (Srivastava et al., 2005a).

Carbon dioxide can be utilized as an oxygen source or a mild oxidant (Noh et al., 2000). It can be used as an alternate medium or solvent (Song, 2006), as a supercritical (sc) fluid (Hutchings, 2009) and as a carbon source. It can be used based on its unique chemical properties to be incorporated with high 'atom efficiency' such as in carboxylation synthesis or in catalyst synthesis (Song, 2006). Hutchings (2009) used supercritical CO_2 as an anti-solvent for the preparation of Au/sc CO_2 and sc-VPO catalysts. The catalysts were tested in many applications, which have resulted in high activity.

1.2.1 The use of CO_2 as C1 building block

The growing concern about the environmental impact of CO_2 emission, have triggered industrialist, researchers and academicians to synthesize organic molecules from CO_2 . Currently, CO_2 has been used in various industrial applications such as chemical, pharmaceutical, foodstuff, beverage, healthcare, environment, pulp and paper, electronics, metal industry, laboratories and analysis, safety and others (Song, 2006).

Among these industries, the application of CO₂ as C1 raw material in the chemical industry has created much attention lately. It has been reported that approximately 110 million metric tonnes of CO₂ is currently used on a yearly base (Peters et al., 2011) in the chemical industry.

Carbon dioxide plays a versatile role in the process of various chemical transformations such as in the production of urea, methanol (Huo et al., 2012), salicylic acid (Iijima and Yamaguchi, 2008), formic acid (Leitner, 1995), cyclic carbonates (Darensbourg et al., 1998), copolymers, polymer building blocks and fine chemicals. Figure 1.2 shows an overview of some of the possible chemical transformation that can be carried out using CO₂ as the C1 source.

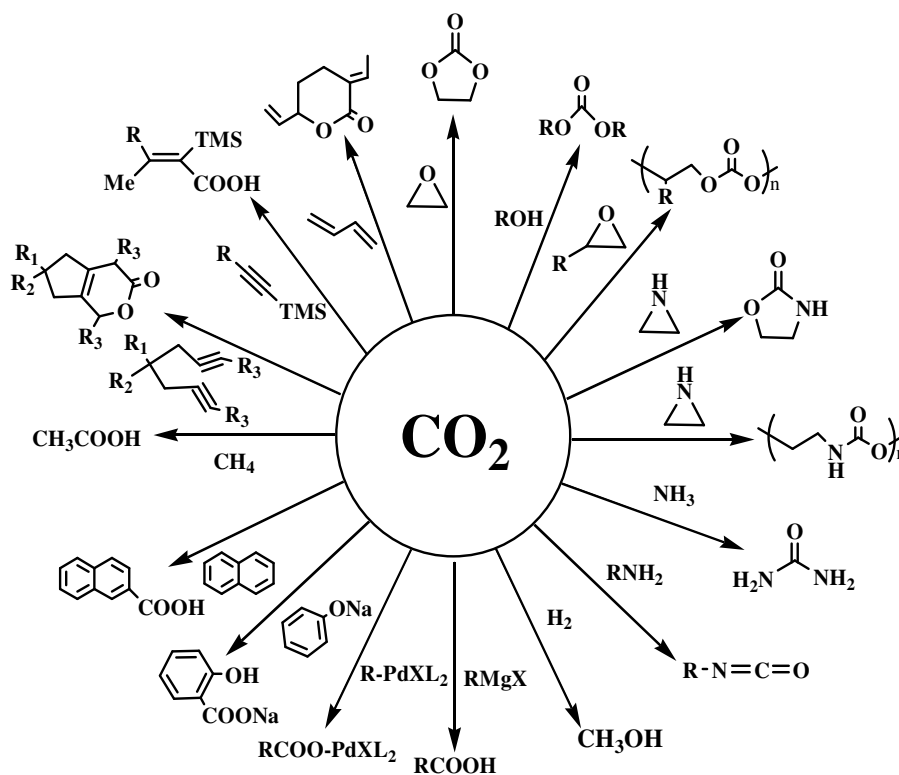


Figure 1.2: A summary of organic transformations using CO₂.

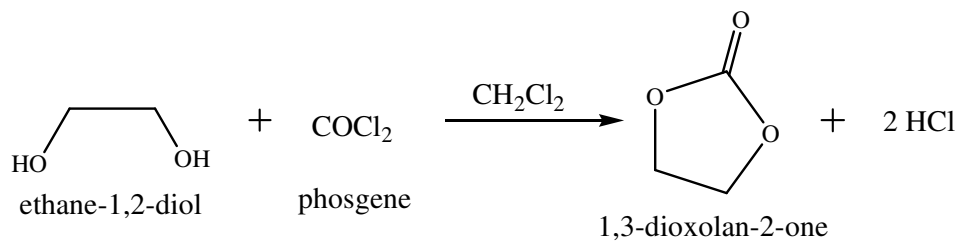
Among the chemicals produced, urea is one of the largest-volume industrial example of converting CO₂ into value-added products. More than 100 million tonnes (Mt) of urea are produced worldwide yearly (Aresta and Dibenedetto, 2007). The urea is synthesized from ammonia and CO₂ and used as fertilizer and also in producing various types of polymers, such as melamine and urea-formaldehyde resin. Salicylic acid is produced from phenol and CO₂ via the Kolbe-Schmitt reaction (Kosugi et al., 2003). The product is used to produce acetyl salicylic acid which is known as aspirin, a commonly used medicine to thin the blood.

1.2.2 Synthesis of cyclic carbonate

The production of cyclic carbonate from the cycloaddition reaction has been well established since 1950s (Metcalf et al., 2013). The cyclic carbonates are colourless, odourless and biodegradable (Ghosh et al., 2010). The cyclic carbonates are used industrially as aprotic polar solvents (Khoshro et al., 2013), additives and as monomers for polymer synthesis too (Dharman et al., 2010). In addition, it has been used in electrolytic materials such as secondary batteries (lithium batteries) (Zalomaeva et al., 2013), resins, cleaning, cosmetics and personal care products (Jutz et al., 2008).

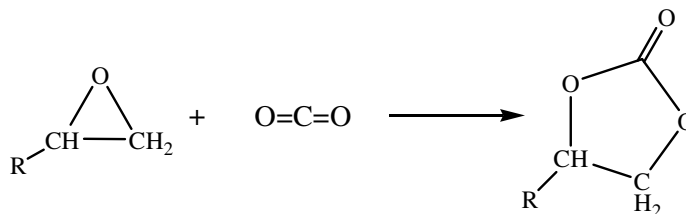
Cyclic carbonates are used as intermediates for pharmaceutical and biomedical fine chemical synthesis too (Zhou et al., 2008). In the agricultural industry, cyclic carbonates are used in the synthesis of herbicides and disinfectants (Aresta et al., 2003). In addition, cyclic carbonates play an important role as an intermediate for the synthesis of fuel additives (Sibaoui et al., 2009).

Traditionally, cyclic carbonates were synthesized by reacting phosgene with ethane-1,2-diol in the presence of excess amounts of dichloromethane as a solvent. At the end of the reaction, hydrochloric acid was produced as a by-product which is harmful to human being (Aresta et al., 2003) and the environment. The conventional synthesis method of organic carbonates is shown in Scheme 1.1.



Scheme 1.1: Synthesis of organic carbonate through conventional method.

By considering the economic value and possible toxicity due to the use of phosgene and with the rising demand of the cyclic carbonates in the chemical industry, CO₂ seems to be a natural choice to replace phosgene. Cyclic carbonates can be synthesized via cycloaddition of CO₂ with epoxides. The CO₂ can be incorporated into the epoxides without formation of by-products (Du et al., 2005). However, due to the inert nature of CO₂, its activation and incorporation into epoxide still remains ambitious (Barbarini et al., 2003) and has stimulated the study of various types of catalysts for the activation of CO₂. The cycloaddition of CO₂ to epoxide is shown in Scheme 1.2.



Scheme 1.2: Cycloaddition of CO₂ to epoxide forming cyclic carbonate.

1.3 Role of catalysts in the production of cyclic carbonates

Catalyst contains “active sites”, which are able to affect the kinetics of chemical reactions and make reactions go faster by reducing the activation energy. Thus, the main recipe to increase the yield of cyclic carbonates from cycloaddition between CO₂ and epoxides is by using catalyst. A wide range of homogeneous and heterogeneous catalysts have been developed to catalyze the so-called CO₂ fixation process. Homogeneous catalysts, such as CoCl₂/onium salt (Sibaouih et al., 2009), diimine Ru(II) complex (Ulusoy et al., 2009), Al-salen-PEA (Alvaro et al., 2005), betaine-based quaternary ammonium ion and carboxylic acid (Zhou et al., 2008), DMF (Kawanami and Ikushima, 2000, Jiang and Hua, 2006), SnCl₄-organic base (Jing and Nguyen 2007), Au/Fe(OH)₃-ZnBr₂/Bu₄NBr (Wang et al., 2009), ionic liquid-highly cross linked polymer (Xie et al., 2007), BrBu₃PPEG₆₀₀PBU₃Br (He et al., 2009), cellulose/KI (Liang et al., 2011) and Au/R201 (Xiang et al., 2009) have been studied.

Several heterogeneous catalysts, such as metal oxides; MgO (Bhanage et al., 2001, Yano et al., 1997), Nb₂O₅ (Aresta et al., 2003), Mg-Al oxide (Yamaguchi et al., 1999), guanidine-MCM-41 (Barbarini et al., 2003), Adeine-Pr-Al-SBA-15 (Srivastava et al., 2006a), Cr-salen-SiO₂ (Alvaro et al., 2004), Mn-salen- SiO₂ (Jutz et al., 2008), CIAIPC-MCM-41 (Lu et al., 2002), as-synthesized MCM-41 (Srivastava et al., 2006b), Ti-SBA-15-Pre-Ade (Srivastava et al., 2005a), 3-(2-hydroxyl-ethyl)-1-propyl imidazolium bromide-SBA-15 (Dai et al., 2010) and zeolite based organic-inorganic hybrid catalysts (Srivastava et al., 2005b) have also been investigated.

Both homogeneous and heterogeneous catalysts have their own advantages and disadvantages. Homogeneous catalyst usually gives higher catalytic activity and selectivity in comparison to heterogeneous catalyst. In heterogeneous catalyst the selectivity is a major problem. In heterogeneous processes mixture of products are obtained due to the nature of the solid support as well as the active site. In some cases, heterogeneous catalysts have requires the use of co-catalyst to enhance its catalytic activity (Srivastava et al., 2005b).

Homogeneous catalysts are less preferred in the industry due to the catalyst-product separation difficulty (Bhanage et al., 2001), which may require more energy and time, but this results in decomposition of the catalysts (Zhou et al., 2008). Therefore, heterogeneous catalysts are far more suitable for large scale industrial synthesis. It can be easily separated from the reaction products and regenerated for subsequent reuse (Alvaro et al., 2005). However, it is important to design and synthesize more efficient heterogeneous catalysts due to the demand for environmentally friendly technologies (Adam et al., 2011b, Adam et al., 2012b).

1.3.1 Heterogeneous ionic liquid catalyst

The development of environmentally benign catalyst for chemical transformation of CO₂ into useful compounds is of vital importance from a green chemistry standpoint. Ionic liquid (IL) is known to be a good reaction media which contributes to its growing importance over the past century (Jutz et al., 2010). In 2003, ILs were widely used in the industry as a solvent as well as a catalyst for the production of useful chemicals (Yang et al., 2011).

In general, the ILs are very useful due to the nature of the anion and cation ($X^- Y^+$) in the compound with melting point less than 100 °C. In comparison to homogeneous IL catalysts, heterogeneous IL catalysts has important physical and chemical features such as non-volatility, non-flammability, good thermal stability, wide liquid temperature ranges and high solvation interaction with both polar and non-polar compounds (Han et al., 2011, Kim et al., 2014).

Several chemical reactions have been catalyzed with homogeneous ILs resulting in high activity and selectivity. However, the system suffers from a major separation and recovery problem. Heterogeneous IL catalysts prepared by grafting ILs onto a solid support such as silica (Han et al., 2011), polymer (Xie et al., 2007, Siewniak et al., 2014), graphite oxide (Luo et al., 2015) or carbon nanotubes (CNT) (Han et al., 2012b) via anchoring agent tends to be recoverable, regenerable and reusable. More recently, multiwall carbon nanotubes (MWCNT) supported imidazolium-based IL was successfully prepared and utilized for the synthesis of various cyclic carbonates (Han et al., 2012b).

It has also been reported that ILs containing zinc tetrahalide anion, exhibits higher performance towards the cycloaddition reaction (Lee et al., 2012). Zhu et al. (2007) reported that choline chloride/urea provide excellent results in the cycloaddition reaction because of the presence of a hydroxyl group in choline chloride. They have proposed that most of the ILs considered as promising heterogeneous catalysts are those containing a quaternary ammonium ion together with a halide anion, -OH or a -COOH group.

The silanol (Si-OH) group in silica supports aminopyridinium halide catalyst which acts as weak Brønsted acid to activate the epoxide. The silanol synergistically enhances the reaction between carbon dioxide with epoxide to form cyclic carbonates under atmospheric pressure (Motokura et al., 2009).

1.4 Factors influencing the production of cyclic carbonates

The production of cyclic carbonates not only depends on the usage of catalyst, but on other reaction parameters such as temperature, pressure and solvent as well. These parameters should be studied to attain high yield of product. Basically, the condition varies depending on the type of epoxide and the catalyst. Table 1.1 summarizes most of the studies carried out for cycloaddition of CO₂ to styrene oxide (SO) on various types of catalysts.

Based on the Table 1.1, it can be concluded that, the performance of the metal oxide catalysts is not satisfactory. Much higher catalytic activities were observed over mixed metal oxides or mixed metal-nonmetal oxides. In some instances, the presence of co-catalyst and solvent are the main disadvantage with respect to “green chemistry” requirements. Compared to the homogeneous catalysts, heterogeneous catalysts such as supported ionic liquid showed better activity and selectivity in cycloaddition reactions. In most studies, the yield of respective product was higher since the active sites of the catalyst contain both acid and base bifunctional groups which could help synergistically activate the epoxide and CO₂ respectively. However, many parameters determine the activity of the catalyst. Therefore, it becomes important that rational design of novel catalytic systems should be supported by a rich experimental activity.

Table 1.1: Catalytic activity studies of cycloaddition of CO₂ to styrene oxide using various homogeneous and heterogeneous catalysts.

Catalyst ^a	Reaction conditions				Reaction results			References
	Solvent or co-catalyst	P _{CO2} (bar)	Temp (°C)	Time (h)	Yield (%)	Selectivity (%)	Conversion (%)	
MgO	DMF	80	150	15	15.8	17.2	92.3	(Bhanage et al., 2001)
MgO	DMF	20	135	12	60.0	-	-	(Yano et al., 1997)
Nb ₂ O ₅	DMF	50	135	12	80.0	-	-	(Aresta et al., 2003)
Mg-Al-Oxide	DMF	5	100	15	90.0	97.8	-	(Yamaguchi et al., 1999)
DMF	-	79	150	15	85.0	-	-	(Kawanami and Ikushima, 2000)
Guanidine-MCM-41	CH ₃ CN	50	140	70	90.0	92.0	-	(Barbarini et al., 2003)
Al-SBA-15- <i>pr</i> -Ade	-	6.9	120	4	88.9	94.6	94.0	(Srivastava et al., 2006a)
Cr-salen-SiO ₂	CH ₂ Cl ₂	100	80	6	74.0	100	-	(Alvaro et al., 2004)
Mn-salen-SiO ₂	-	35 ^b	140	3	95.0	-	-	(Jutz et al., 2008)
ClAlPc-MCM-41	n-Bu ₄ NBr	40	110	2	384 ^c	-	-	(Lu et al., 2002)
Al-salen-PEA	n-Methyl imidazole	100	80	15	78.0	87.6	89.0	(Alvaro et al., 2005)
Betaine based salt ^d	-	80	140	8	96.0	-	-	(Zhou et al., 2008)
Au/R201	-	40	150	4	92.5	97.0	95.4	(Xiang et al., 2009)
MCM-41 ^e	CH ₃ CN	6.9	120	8	-	98.2	88.4	(Srivastava et al., 2006b)
	-	6.9	120	8	-	95.2	93.7	(Srivastava et al., 2006b)
Zn/Ps-IL[Br]	-	30	120	8	97.5	-	-	(Qiao et al., 2009)
SalenRu(II)(PPh ₃) ₂ /PTAT	EtOH ^f	8.3	70	2	92.0	-	-	(Jing et al., 2007)
CoCl ₂ /onium salt	CH ₂ Cl ₂	15	120	1	1238 ^c	-	-	(Sibaouih et al., 2009)

Ti-SBA-15- <i>pr</i> -Ade	CH ₃ CN	6.9	120	8	-	87.0	79.8	(Srivastava et al., 2005a)
	-	6.9	120	8	-	94.6	94.0	(Srivastava et al., 2005a)
Diimine Ru(II) complex	-	16	100	2	73.1	-	-	(Ulusoy et al., 2009)
IL-polymer	-	60	110	7	79.1	-	-	(Wang et al., 2009)
Cellulose/KI	-	20	110	9	98.0	-	-	(Liang et al., 2011)
HEPIMBr	-	20	120	2	99.6	-	99.8	(Dai et al., 2010)
IL tetrabutylammonium chloride	-	9.7	100 ^g	0.5	97.9	-	-	(Dharman et al., 2010)
Au/Fe(OH) ₃ -ZnBr ₂ /Bu ₄ NBr	-	40	80	10	53.0	-	-	(Wang et al., 2009)
Co(III) complex	DMAP	20	120	3	85.8	-	-	(Ghosh et al., 2010)
SLPC	Toluene	45	150	6	84.8	-	-	(Jagtap et al., 2006)
Co(III) Porphyrin/DMAP	CH ₂ Cl ₂	20.7	120	4	97.0	-	-	(Paddock et al., 2004)
MNP-Co-Porphrin	CH ₂ Cl ₂	10	25	36	48.7	-	-	(Bai et al., 2011)
M(TTMAPP)I ₄ (X) M=Co;X= OAc	-	6.7	80	36	62.5	-	-	(Bai et al., 2010)
Bis-(phenoxyiminato) cobalt(III)/lewis base	CH ₂ Cl ₂	10	145	1	600/640 ^c	-	-	(Sibaouih et al., 2009)
Metal porphyrin/phenyltrimethyl-ammonium tribromide	-	6.9	20	10	20.0	-	-	(Jin et al., 2007)
SnCl ₄ -organic base	-	3.5	75	1.5	96.0	-	-	(Jing and Nguyen 2007)
DMF	-	50	110	15	8.0	-	-	(Jiang and Hua, 2006)
Zeolite-based- organic-inorganic	-	6.9	120	8	-	92.8	98.0	(Srivastava et al., 2005b)
CS-[BuPh ₃ P]Br	-	25	120	6	96.9	97.4	99.5	(Jing-Xian et al., 2014)

[Ph ₃ PC ₂ H ₄ COOH]Br		25	130	3	99.5	99.8	99.7	(Wei-Li et al., 2014a)
ChI	EtOH	10	85	6	99.0	94.0	-	(Amaral et al., 2013)
KI/PDA		20	120	5	34.7	99.0	35.0	(Yang et al., 2014)
[P-Im-C ₄ H ₈ Ph ₃ P]Br ₂		25	130	4	99.3	99.8	99.5	(Wei-Li et al., 2014b)
SBA-15-IL1Br		20	110	3	80.0	99.0	80.8	(Cheng et al., 2013)
Si-Imi		6	130	10	76.6	97.0	79.0	(Sankar et al., 2015)
Cr-CMP		30	100	2	96.3	-	-	(Xie et al., 2014)
PDDA-Br		25	100	12	92.9	97.8	95.0	(Song et al., 2014)
PPN(I)	ZnI ₂	1	100	7	89.0	94.7	94.0	(Motokura et al., 2014)
OXCNT-(CH ₂)(Me) ₃ N ⁺ Cl ⁻		20	110	6	22.0	96.0	23.0	(Baj et al., 2014)
P-DVB-HEImBr		20	140	5	98.9	100	98.9	(Dai et al., 2013)
PS-hexyl-MeI		12	120	12	96.7	-	-	(Lee et al., 2014)
PS-TBMAC	ZnI ₂	9	110	2	71.0	99.0	70.3	(Siewniak et al., 2014)

^a Abbreviations. *pr*: 3-chloro or 3-aminopropyltriethoxysilane; Ade: adenine; CIAIPc: aluminium phthalocyanine; PEA: poly(ethylene glycol bismethacrylate); PTAT: phenyltrimethylammonium tribromide; HEPIMBr: 3-(2-Hydroxyl-Ethyl)-Propylimidazolium Bromide; SLPC: supported liquid phase catalyst; MNP: magnetic nanoparticle; M(TTMAPP)₄(X): Bifunctional metalloporphyrins; CS: chitosan; ChI: choline iodide; PDA: polydopamine; CMP: conjugated Microporous polymer; Imi: imidazole; PDDA-Br: polydiallyldimethylammonium bromide; PPN(I): 4-Pyrrolidino-(3-(trimethoxysilyl)propyl)pyridinium Iodide; CNT: carbon nanotubes; PS: Polystyrene-supported quaternized ammonium salt; PS-TBMAC: polymer-supported tributylmethylammonium chloride.

^b molar ratio of CO₂ to styrene oxide.

^c Turnover frequency (h⁻¹) value.

^d containing quaternary ammonium ion and carboxylic acid group.

^e as-synthesized MCM-41 (without calcination).

^f recrystal with ethanol.

^g Microwave assisted.

1.4.1 Influence of temperature

Temperature is one of the important parameters in a catalytic reaction. An effective collision happens during the reaction with sufficient speed, energy and force to break bonds in the colliding molecules. Therefore, the yield of the product is strongly dependent on the reaction temperature. Aresta et al. (2003) studied the influence of temperature on the formation of styrene carbonate (SC) from styrene oxide and CO₂ with Nb₂O₅ as a catalyst. The reaction did not yield any product below 100 °C. However, the product yield increased to 80 % as the temperature rose to 135 °C. This indicates that a slight change in the temperature can influence the product formation in a reaction.

Jutz et al. (2008) studied the influence of the reaction temperature on the performance of Mn(salen)Br catalyst by utilizing a broader range of temperature. Maximum yield was obtained at 160 °C, but reduced dramatically at a higher temperature. This behavior was accounted to phase distribution changes of the reactants which normally occur at higher temperatures. Zhou et al. (2008) reported that at 140 °C, the yield of propylene carbonate (PC) was 98 % and reduced to 78 % at 150 °C. The decrease in the yield was possibly due to the occurrence of side reactions, which happens after the entire propylene oxide (PO) was converted at the higher temperature. Bai et al. (2010) reported that the increase in the temperature caused a decrease in PC yield, due to the decomposition of the catalyst at the higher temperature. Qiao et al. (2009) explained that, SO is difficult to convert to SC compared to other epoxides due to its less reactive β-carbon atom. Thus, it requires a longer reaction time and higher temperature.

He found that the temperature of 120 °C (98 %) was the optimum condition compared to 130 °C (~80 %) and 140 °C (~95 %). However, the reaction temperature for optimal performance is dependent on the nature of the catalyst employed and it is widely known that cycloaddition reaction is an exothermic process (Dai et al., 2010).

Recently, Lee et al. (2014) studied the effect of reaction temperature on the cycloaddition reaction between ally glycidyl ether (AGE) and CO₂ using PS-*hexyl*-MeI at 12 bar of total pressure. They found that the yield of allyl glycidyl carbonate (AGC) increased from 80 to 140 °C; however, it decreased at 160 °C. The decreased was due to the formation of oligomers and some by-products such as 3-allyloxy-1,2-propanediol. Zhong et al. (2014) investigated the effect of temperature in the range of 120 °C to 160 °C on the propylene carbonate yield in the presence of little (0.78 mmol) and large amount (13.7 mmol) of DMF. They concluded that, the large amount of DMF used was favorable to decrease the reaction temperature.

1.4.2 Influence of pressure

The pressure of the carbon dioxide has been established as one of the most crucial factor affecting the cycloaddition reaction with epoxide (Qiao et al., 2009), since CO₂ acts as a reactant and as a reaction medium simultaneously (Jutz et al., 2008). There are two phases in the reaction system, where the top phase is rich with CO₂ and the bottom phase is rich with epoxide. According to Xie et al. (2007), the CO₂ acts as a reactant and favors the reaction when the bottom phase is under high pressure.

However, this condition is not favorable to the reaction at the high pressure (120 bar), because the concentration of epoxide (PO) which acts as a reactant, at the bottom phase decreases. Therefore, at high pressure, more epoxide can be extracted into CO₂ rich phases; hence greatly reduces the reaction rate.

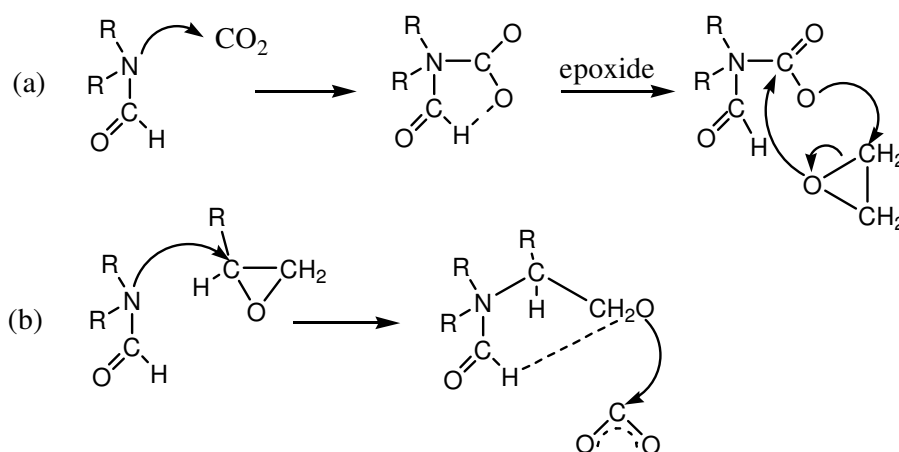
Ghosh et al. (2010) reported that at lower pressure (7 bar) the catalyst retains sizable activity (TOF: 312 h⁻¹) and with increasing pressure up to 20 bar higher TOF value of 351 h⁻¹ was observed. However, the pressure higher than 20 bar diminishes the overall activity of the catalyst. This is due to the decrease in polarity of the reaction mixture and solubility of the catalyst in the reaction mixtures is lowered. Qiao et al. (2009) studied the influence of CO₂ at different pressure ranges, e.g., mild pressure (15 bar), medium pressure (80 bar) and supercritical pressure (140 bar) for the CO₂ cycloaddition with SO. By increasing the pressure to more than 60 bar, they observed a negative effect on the reaction, where, both yield and conversion reduced tremendously. This was due to changes in phase from gas to supercritical fluid, where a part of SO dissolves in the supercritical CO₂ and decrease the amount of reaction substrate in liquid phase where the reaction occurs.

Wang et al. (2009) observed, that the introduction of too much CO₂ dissolves in SO or “liquefies” the formation of CO₂-SO complex, and retards the interaction resulting in a lower conversion. Lately, similar results were also reported where the introduction of higher pressure of CO₂ dissolved in the PO and becomes an unfavorable factor due to the difficulty of separating CO₂ and PO, and inhibit the reaction between PO and catalyst, thus resulting in lower yield (Xiao et al., 2014, Wei-Li et al., 2014b).

Xiang et al. (2009) reports that many oligomers were produced as side products at high pressure. In a solvent-less reaction with (PO and SO) and CO₂, Jutz et al. (2008) reported that a ratio of 1:4 (epoxide: CO₂) was found to be optimum compared to a ratio of 1:16 for both epoxides. They also studied the phase behavior to investigate the influence of the fluid phases present in the catalytic reaction.

1.4.3 Influence of solvent

The synthesis of cyclic carbonate is carried out in the presence of solvents too. The solvent plays a vital role in removing the carbonaceous deposits from the catalyst surface and keeps the reaction system clean. Thus, the catalysts life is prolonged significantly (Bhanage et al., 2001). Aresta et al. (2003) demonstrated that, *N,N*-dimethylformamide (DMF) alone yields 34.7 % of SC at 50 bar. They also found that, the amide group acts as good promoter. Dimethylacetamide (DMA) produced 28 % of SC yield at 50 bar, 135 °C and for 12 h without the usage of any catalyst. The role of DMF in the cycloaddition of epoxides is shown in the Scheme 1.3.



Scheme 1.3: Role of DMF in the cycloaddition of epoxides (Aresta et al., 2003).

According to the mechanism, the role of amide is to increase the nucleophilicity of the relevant oxygen atoms in either epoxide or CO₂. To enhance the activity of the reaction, methylene chloride or 1,2-dichloroethane was added as an additive to DMF along with Nb₂O₅ catalyst. It was suggested that, methylene chloride could contribute to stabilize polar or ionic intermediates through the C^{δ-}-H^{δ+}, C^{δ+}-Cl^{δ-} dipoles. Additives such as tetrachloromethane and ethanol when used together with DMF, shows a co-operative solvation effect.

In the case of dimethylsulfoxide (DMSO), several side products were observed in the presence of a catalyst. In the investigation, xylenes and toluene did not yield any product without catalyst. However, for xylenes, a very poor yield was observed in the presence of a catalyst. Kawanami and Ikushima (2000) used DMF as a catalyst and solvent under supercritical conditions, where CO₂ with epoxide were dissolved in DMF-scCO₂. Under this condition, the viscosity of the solution was reduced and the diffusion rate was increased when compared with the DMF of the liquid phase. Recently, Zhong et al. (2014) utilized DMF as co-catalyst together with ZnBr₂ as a catalyst for cycloaddition reaction of CO₂ to PO. They have described, DMF acted as solvent as well as CO₂ activator. A 100 % selectivity to PC were registered at 150 °C, 30 bar within very short reaction time of 10 min. Alvaro et al. (2004) used about 0.4 mL dichloromethane or dimethyl carbonate as a co-solvent to increase the solubility in the medium of SO and used the base as a co-catalyst. They have observed 70 % conversion with 100 % selectivity under supercritical condition (100 bar, 80 °C) in a 50 mL reactor for 6 h in the presence of a Cr-salen base catalyst.

A new approach was taken by Jiang and Hua (2006) in order to study the effect of various solvents during the synthesis of chloropropene carbonate from epichlorohydrin. They found that, protic alcohols such as methanol and ethanol were good solvents for the formation of chloropropene carbonate, which were 90 % and 82 % in methanol and ethanol respectively. However, high molecular weight of benzyl alcohol resulted in a decreased productivity (12 %). Nevertheless, they observed a maximum yield of > 99 % at 110 °C for 20 h with DMF as the solvent.

1.5 The mechanism of cycloaddition of CO₂ to epoxides

1.5.1 Ring opening of epoxide

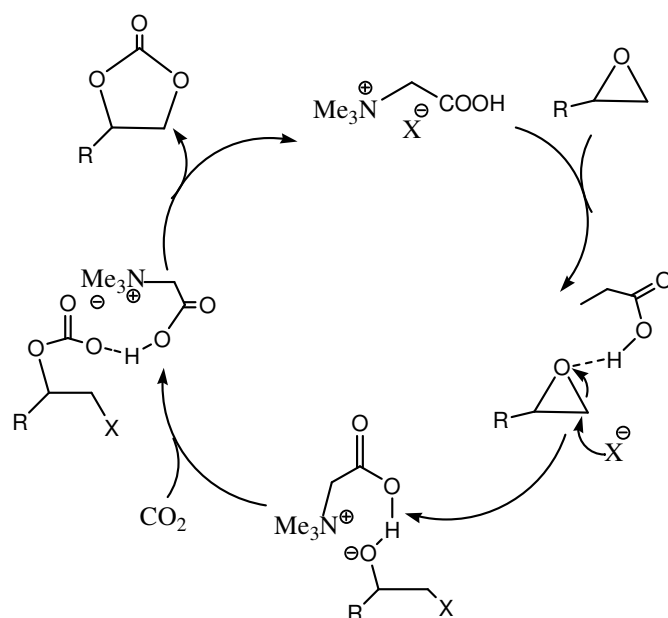
Basically, the ring opening of the epoxide is described in terms of two pathways; (i) Lewis-acid catalyzed cleavage and (ii) Lewis-base catalyzed cleavage. Bu et al. (2007) found that the ruthenium complex ((2,2'-bipy)RuCl₃(CH₃OH)) together with cetyltrimethylammonium chloride (CTAC) catalyzes the reaction of CO₂ with propylene oxide (PO) which forms a 100 % yield of propylene carbonate.

In this complex, Ru acted as a Lewis-acid to activate the PO to form adduct of Ru-PO. However, in this case they found that the adduct itself was not able to open the PO ring. The addition of CTAC is vital, in which it performs a crucial role in enhancing the ring opening intermediate. The chloride anion (Lewis-base) in CTAC attacks the less sterically hindered carbon atom to open the epoxide ring while forming the oxy anion species.

Bai et al. (2010) found that the bifunctional metalloporphyrins $M(\text{TTMAPP})\text{L}_4(\text{X})$ ($M = \text{Co}, \text{Fe}, \text{Mn}$ and Cr ; $\text{X} = \text{OAc}, \text{CF}_3\text{COO}, \text{CCl}_3\text{COO}, \text{OTs}, \text{Cl}, \text{Br}$ and I) were highly efficient catalysts for the cycloaddition reaction of PO and CO_2 . They observed that, metal acts as a Lewis acid center to catalyze the reaction. The activity order of the metal was $\text{Co} > \text{Mn} > \text{Fe} > \text{Cr}$. The catalytic activity order in the presence of cobalt porphyrin and other different counterions was $\text{OAc}^- > \text{I}^- > \text{Cl}^- > \text{Br}^- > \text{OTs}^- > \text{CF}_3\text{COO}^- > \text{CCl}_3\text{COO}^-$.

Barbarini et al. (2003) reported that, MCM-41-supported guanidine catalysts which contains hydroxyl groups on the arm and silanols on the support surface. Both hydroxyl and silanol groups could activate the epoxide by H-bond formation but there were no evidence to prove this hypothesis. Zhou et al. (2008) investigated the synthesis of cyclic carbonate over betaine (HBetX) and choline cation (ChoX) catalysts. They found that either the hydroxyl group or the carboxylic acid group affects the activity of the catalysts. Besides that, they reported the comparison among the anion such as Cl^- , Br^- , I^- , BF_4^- and PF_6^- . The yield for PC synthesis decreased in the order of $\text{Cl}^- > \text{BF}_4^- > \text{PF}_6^-$. Moreover, the leaving ability of the anions plays an important factor and their activity increases in the order of $\text{I}^- > \text{Br}^- > \text{Cl}^-$. The use of better nucleophilic anions will attack the epoxide ring effectively to form a reactive intermediate.

The carboxylic acid group was found to be more useful, where it shows a cooperative effect with halide anions to activate the ring opening of epoxides than hydroxyl group due to the stronger Brønsted acid and hydrogen bonding donor. The reaction mechanism for the cycloaddition reaction is shown in Scheme 1.4.



Scheme 1.4: The assumed reaction mechanism for the cycloaddition of epoxide with CO₂ catalyzed by HBetX (Zhou et al., 2008).

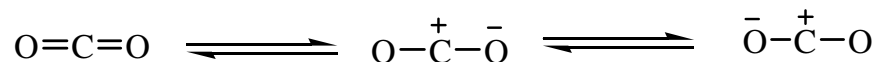
Qiao et al. (2009) described that ZnX, X= Br⁻, Cl⁻, BF₄⁻, PF₆⁻ immobilized on soluble imidazolium-styrene copolymers was a suitable catalyst for the CO₂ cycloaddition to SO. Among the catalyst investigated, Zn/PS-IL[Br] was the most efficient, which gave 97.5 % yield with a TOF of 3800 h⁻¹. Although, this catalyst was considered as homogeneous, but it could be reused three times due to its immiscibility with ethanol without significant loss in activity. The Zn/PS-IL[Cl] showed a product yield of only 35 %, with TOF of 1300 h⁻¹. The authors suggested that, this could be due to the stronger nucleophilicity of Br⁻ than that of Cl⁻ under the reaction conditions. Jing et al. (2007) suggested that the high activity of the catalyst could be attributed to the good leaving group of Br⁻.

Dai et al. (2010) reported that 3-(2-hydroxyl-ethyl)-1-propyl imidazolium bromide-SBA-15 (HEPIMBr) as an efficient catalyst for the synthesis of cyclic carbonates under mild conditions in a solvent-free environment and in the absence of a co-catalyst. They proposed that, the intermediate formation occurred when the H atom of the hydroxyl group coordinated with the O atom of epoxide through hydrogen bonding. Then, the halide anion makes a nucleophilic attack on the sterically less hindered β -carbon atom of the epoxide, due to the polarization of the C-O bonds and the ring opening of epoxide occurs concurrently.

Recently, Jing-Xian et al. (2014) reported biopolymer chitosan-grafted quarternary phosphonium ionic liquid (CS-[BuPh₃P]Br) as an excellent catalyst for the cycloaddition of epoxide with CO₂. They have proposed that the facilitation of ring opening of epoxides is due to a combined result of polarization. The bromide anion of the catalyst opens the epoxy ring, which was activated by the hydroxyl groups and phosphonium cation through hydrogen bonding as well as electronic interaction. A similar catalysts were developed by Wei-Li et al. (2014a) using phosphonium-based ionic liquid functionalized with carboxyl, hydroxyl and amino as a functional groups. Similarly, the epoxide ring is opened via the hydrogen bonding between the H atom of functional group and the O atom of epoxide, resulting in polarization of epoxide C-O bond and formation of intermediate. Then, there is nucleophilic attack of Br⁻ on the less sterically hindered β -carbon atom of epoxide, facilitating opening of epoxy ring and formation of another intermediate.

1.5.2 Activation of CO₂

Carbon dioxide chemical fixation is both important and possible due to two potential activation sites as shown in Scheme 1.5.

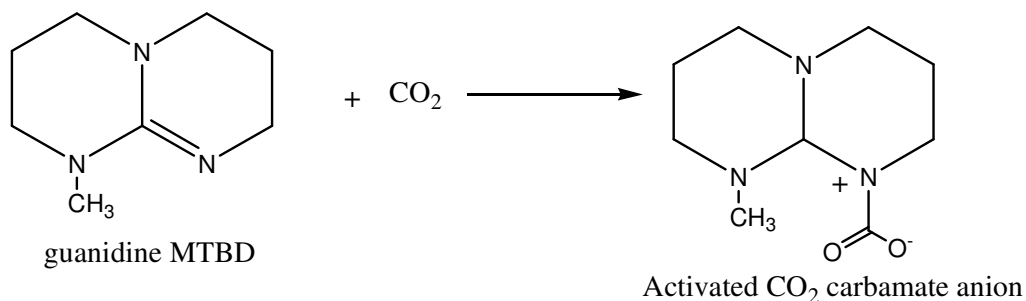


Scheme 1.5: The carbon and oxygen atoms act as Lewis acid and Lewis base respectively. Both are potential activation sites.

Carbon dioxide could be catalytically activated into valuable chemical when it reacted with the molecules containing an electron donor or an active hydrogen group. A catalyst plays an important role to activate the CO₂ for its participation in the chemical reaction to produce the respective cyclic carbonates.

Lu et al. (2002) prepared MCM-41 supported aluminium phthalocyanine complex for the reactions of CO₂ and epoxides and found that the co-catalyst, *n*-Bu₄NBr enhanced the reaction as well as giving high catalytic activity. In their studies, they found that the activation of CO₂ was initiated by the nucleophilic attack of the alcoholate (-OCH₂CH₂Br) at the carbon atom of CO₂, weak interaction between the central metal ion of ClAlPc and the lone pairs of one of the oxygen of CO₂. The catalyst showed a synergistic effect in promoting these reactions via the insertion of CO₂ to the Al-O bond of Pc(Cl)Al-OCH₂CH₂Br to form linear carbonates and it converts into cyclic carbonates by intramolecular substitution of halides.

On the other hand, Barbarini et al. (2003) observed that CO₂ was activated through the formation of the zwitterionic compound (Scheme 1.6), where it later adds to the epoxide via nucleophilic attack.



Scheme 1.6: Hypothesized MTBD-promoted CO₂ activation (Barbarini et al., 2003).

Srivastava et al. (2005a) critically investigated the properties of the catalyst in the activation of CO₂. FTIR spectroscopy was used to identify the structural features of CO₂ in the adsorbed state of the catalyst. The CO₂ reacted with the amine functional group in SBA-15-*pr*-Ade and Ti-SBA-15-*pr*-Ade which was confirmed with the presence of the carbamate bands at 1609 and 1446 cm⁻¹.

Conversion (62.3 %) of epichlorohydrin was obtained after the functionalization of adenine group compared to the bare SBA-15 (1.5 %). This increase in conversion was correlated with the intensity of the band at 1609 cm⁻¹, due to the CO₂ activation at the amine sites, highlighting the importance of such sites for CO₂ activation. In another report, Srivastava et al. (2006a) compared and investigated the importance of the basic sites of the catalysts such as alkyl amines (-NH₂), adenine (Ade), imidazole (Im) and guanine (Gua) in the activation of CO₂.